Journal of Magnetic Resonance **137,** 196–205 (1999)
Article ID jmre.1998.1663, available online at http://www.idealibrary.com on IDEAL®

Resolution in High Field Echo Planar Microscopy

A. M. Peters and R. Bowtell[1]

Magnetic Resonance Centre, School of Physics and Astronomy, University of Nottingham, University Park, Nottingham NG7 2RD, United Kingdom

Received July 23, 1998; revised November 18, 1998

The application of echo planar imaging to NMR microscopy offers a temporal resolution unparalleled by other techniques. However, a major difficulty in imaging at the high field strengths used for microscopy is the effect of local field inhomogeneities caused by magnetic susceptibility effects. This can give rise to both image distortion and signal loss. In addition, the effect of diffusion in the presence of the large imaging gradients gives rise to a broadening of the point spread function and hence loss of true resolution. We compare the sensitivity of two techniques, MBEST and PEPI, to both of these effects. Analytic expressions for the signal in each echo of the two sequences are developed, and the point spread functions for the two techniques are calculated. Using PEPI, we have been able to produce images with an in-plane resolution of 50 μm from a single free induction decay. This technique has been extended to three dimensions allowing the generation of 64^3 images with an isotropic resolution of 80 μm. © 1999 Academic Press

Key Words: **NMR microscopy; EPI; PEPI; diffusion.**

INTRODUCTION

The application of echo planar imaging (EPI) (*1*) to NMR microscopy allows real-time imaging at resolutions of less than 100 μm. This unparalleled temporal resolution makes possible the study of dynamic processes such as diffusion and flow in real time. Extending the technique to three dimensions either by acquiring a number of 2D slices or by adding a phase encoding step along the third axis allows the rapid imaging of whole samples, and the three-dimensional mapping of parameters such as relaxation times in a few minutes.

NMR microscopy experiments are usually carried out at high magnetic field, since the NMR signal and hence signal-to-noise ratio (SNR) in the image increases with increasing field strength (*2*). However, the implementation of EPI at the high field strengths commonly used for microscopic studies presents difficulties associated with susceptibility-induced field distortion. Because of the low frequency per point of the EPI experiment, it is particularly sensitive to these effects. A second difficulty is the effect of diffusion in the presence of the large gradients required to achieve the desired spatial resolution. This gives rise to signal loss which gives a broadening of the point spread function (PSF), thus limiting the achievable resolution.

[1] To whom correspondence should be addressed. Fax: +115 9515166; E-mail: richard.bowtell@nottingham.ac.uk.

SEQUENCES FOR MICROSCOPY

Two related sequences have been considered for application to microscopy, MBEST (*3, 4*) and PEPI (*5*). As can be seen from the MBEST pulse sequence shown in Fig. 1a, following slice selection, a hard 180° RF pulse is used to generate a spin echo. A preexcursion pulse precedes a series of repeated gradient reversals which generate a train of gradient recalled echoes occurring at the center of each gradient pulse. The preexcursion of the blipped (phase encoding) gradient is timed so that the center of *k*-space is traversed at the center of the spin echo. In this way *k*-space is traversed in a raster fashion as shown in Fig. 1b. Alternate lines of data must be time reversed to account for the polarity of the switched gradient under which they were acquired, before the Fourier transform.

The PEPI sequence, shown in Fig. 2a, is a modification of EPI, which uses a series of 180° RF pulses in place of repeated gradient reversals to generate a series of echoes. All of the switched gradient pulses must therefore be of the same polarity, and so time reversal of alternate echoes is not required. However, the action of the 180° RF pulses affects the order of acquisition of *k*-space data, with the center of *k*-space being sampled first, as shown in Fig. 2b. Reordering of the data is therefore required before Fourier transformation. Any dephasing of transverse magnetization due to magnetic field inhomogeneities is periodically refocused by the RF pulses, giving rise to a reduction in related image distortion. Previously, PEPI has been used to investigate fluids in porous media at lower field (0.5 T) and has had particular application in the measurement of flow (*6, 7*).

THEORETICAL COMPARISON

Diffusion Limited Resolution

The image resolution achievable with either of the two techniques described above is ultimately limited by diffusion (*8*). Random motion of the spins under the applied gradients causes an irreversible dephasing of transverse magnetization and consequent signal decay during the ac-

1090-7807/99 $30.00
Copyright © 1999 by Academic Press
All rights of reproduction in any form reserved.

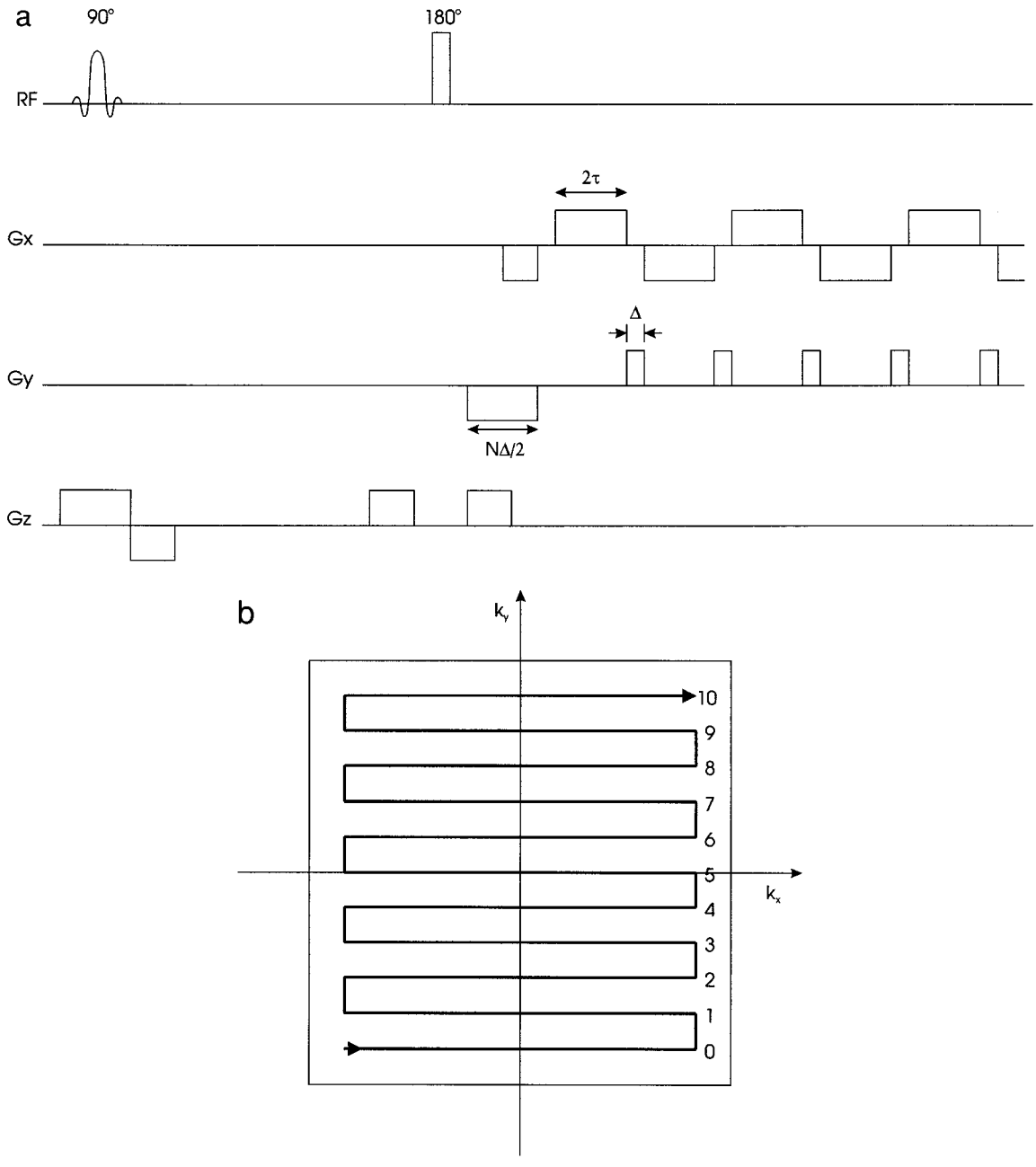

FIG. 1. (a) MBEST pulse sequence as implemented on the microscope system. (b) MBEST *k*-space coverage.

quisition. This signal decay gives rise to an increase in the width of the point spread function and consequent loss of image resolution. In EPI and PEPI, this function is broadest in the phase encode direction, since the signal decay over the whole acquisition is much greater than that during the acquisition of a single echo. It is therefore the PSF in the phase encode direction which limits the resolution of the experiment.

To evaluate the diffusion limit to resolution, it is necessary to calculate the diffusion-induced signal attenuation for each echo in the experiment. The attenuation A at time t caused by diffusion under a gradient $G(t)$ is given by (*9*)

$$A = \exp\left(-\gamma^2 D\left(\int_0^t \left(\int_{t'}^t G(t'')dt''\right)^2 dt'\right)\right), \qquad [1]$$

where D is the diffusion coefficient and γ is the gyromagnetic ratio.

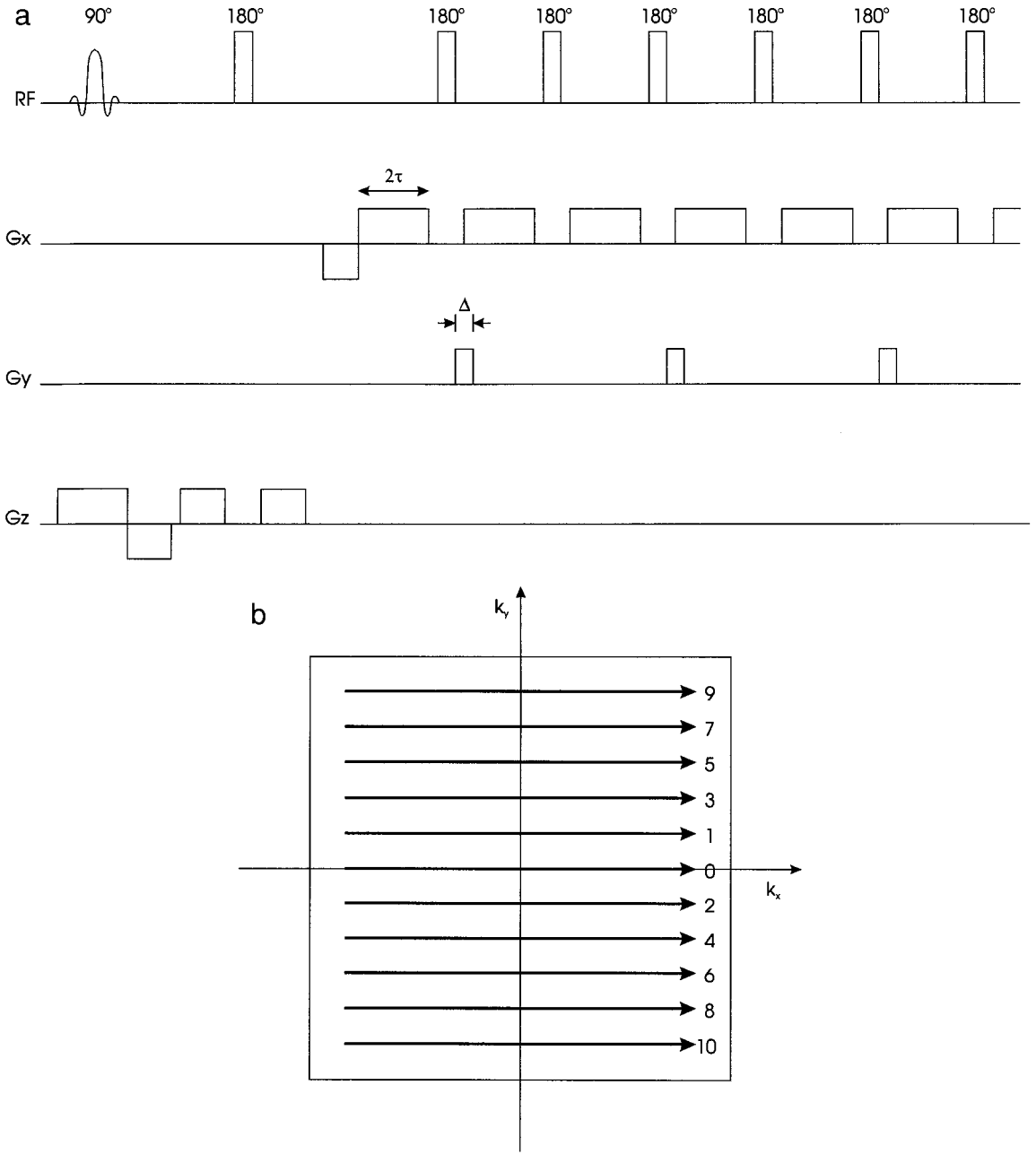

FIG. 2. (a) PEPI sequence as implemented on the microscope system. (b) PEPI *k*-space coverage showing the order of data acquisition.

MBEST. The attenuation of echoes in the MBEST sequence results from the action of both the switched and the blipped gradients. Since these gradients are orthogonal, the effect of each can be considered independently, and combined to give the total attenuation through the sequence.

Considering first the blipped gradient, from the pulse sequence shown in Fig. 1a, it can be seen that the *m*th echo occurs at a time τ_m after the 180° RF pulse given by

$$\tau_m = \frac{N\Delta}{2} + \tau + m(\Delta + 2\tau), \qquad [2]$$

where N is the total number of echoes sampled, Δ is the length of each phase encoding blip, and 2τ is the time between the blips. Evaluating Eq. [1], it can be shown that the attenuation of the *m*th echo due to the blipped gradient of strength, G_y, is

$$A_{bl} = \exp\left(\frac{-\gamma^2 D G_y^2 \Delta^2}{3}\left(\tau m(m+1)(2m+1) + 2\Delta m^3 + \frac{\Delta(N-2m)^3}{8}\right)\right). \qquad [3]$$

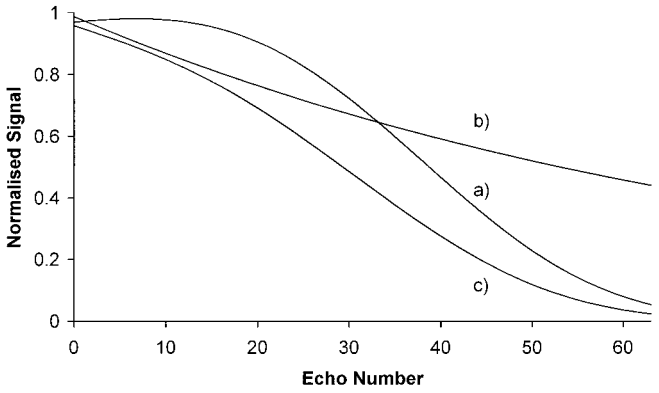

FIG. 3. Signal attenuation during an MBEST experiment with a resolution of 31 μm caused by diffusion under (a) the blipped gradient, (b) the switched gradient and (c) both gradients. Acquisition parameters: gradient strength $G_x = 0.575$ T/m, $\tau = 659$ μs, blipped gradient strength $G_y = 0.092$ T/m, $\Delta = 128$ μs, and $D = 2.2 \times 10^{-9}$ m^2/s. The attenuation due to the blipped gradient includes the effect of the preencoding lobe of duration $N\Delta/2$. As the opposite polarity blips are applied some of this attenuation is removed leading to a peak in the signal amplitude at the 7th echo. This behavior is the same as that previously reported for a standard gradient echo sequence (*9*).

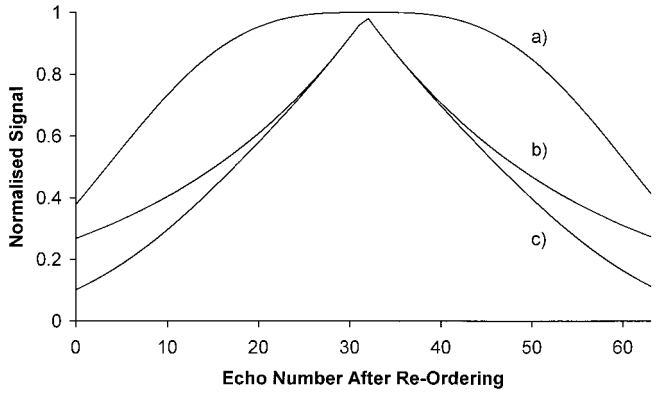

FIG. 4. Signal attenuation during a PEPI experiment with a resolution of 28 μm caused by diffusion under (a) the blipped gradient, (b) the switched gradient, and (c) both gradients. Acquisition parameters: gradient strength $G_x = 0.575$ T/m, $\tau = 729$ μs, blipped gradient strength $G_y = 0.1$ T/m, $\Delta = 128$ μs, and $D = 2.2 \times 10^{-9}$ m^2/s.

The switched gradient can be viewed as a series of repeated units consisting of positive and negative gradient lobes each of amplitude G_x and duration τ, separated by a time Δ. The gradient waveform integrates to zero over each of these units. The attenuation due to the application of one unit can be written as

$$A = \exp\left(\frac{-\gamma^2 D G_x^2}{3}(2\tau^3 + 3\Delta\tau^2)\right). \quad [4]$$

The attenuation of the mth echo due to the switched gradient is therefore given by

$$A_{sw} = \exp\left(\frac{-\gamma^2 D G_x^2}{3}(2\tau^3 + 3\Delta\tau^2)(m+1)\right). \quad [5]$$

Combination of Eqs. [3] and [5] yields the total attenuation through the sequence, the Fourier transform of which gives the PSF. The Rayleigh criterion can then be used to assess the effect that diffusional attenuation has on resolution.

The form of Eqs. [3] and [5] indicates that the exponent describing the signal decay varies with the square of gradient strength and the cube of experimental duration. For the narrowest PSF, and therefore best resolution, it is necessary to use the largest available gradient strengths applied for only as long as is necessary to achieve the desired pixel spacing.

Assuming a 64 $\times$ 64 image matrix, a switched gradient strength of 0.575 T/m, blip duration $\Delta = 128$ μs, equal resolution in the x and y directions, and a sample of water at room temperature ($D = 2.2 \times 10^{-9}$ m^2 s^{-1}), then the Rayleigh criterion is just met when the pixel spacing is 31 μm. The corresponding signal attenuation is shown in Fig. 3. This could be reduced with the use of larger gradients; however, a doubling of the available gradient strength only reduces the diffusion limit to 26 μm, at the expense of a doubling of the acquisition bandwidth. Figure 3 also shows that by the time the center of k-space is sampled, diffusion alone has reduced the signal to 40% of its full value, leading to a marked reduction in the SNR of the image.

PEPI. The phase encoding gradient in PEPI is similar to that for MBEST, except that two echoes are acquired between each gradient blip, and there is no preexcursion. Using Eq. [1] it can be shown that the attenuation of the signal acquired in the lth space between phase encoding blips is

$$A_{bl} = \exp\left(\frac{-\gamma^2 D G_y^2}{6}(\Delta^2 l(2l-1)(l-1) \times (3\Delta + 4\tau) + 2\Delta^3 l^3)\right). \quad [6]$$

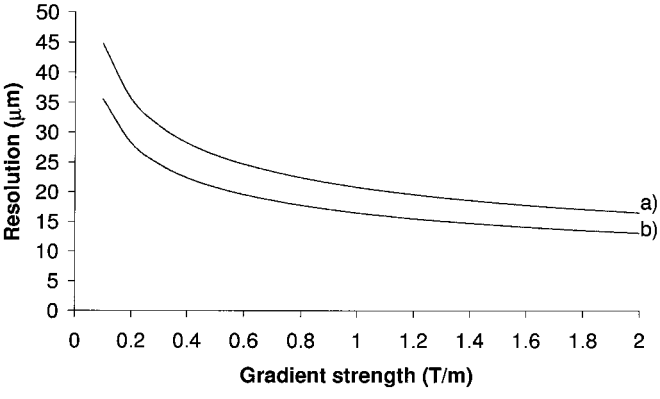

FIG. 5. Graph of maximum possible resolution using PEPI against available gradient stength for a diffusion coefficient of (a) 2.2×10^{-9} m^2 s^{-1} and (b) 1.1×10^{-9} m^2 s^{-1}, assuming $G_x = G_y$ and zero gradient rise time.

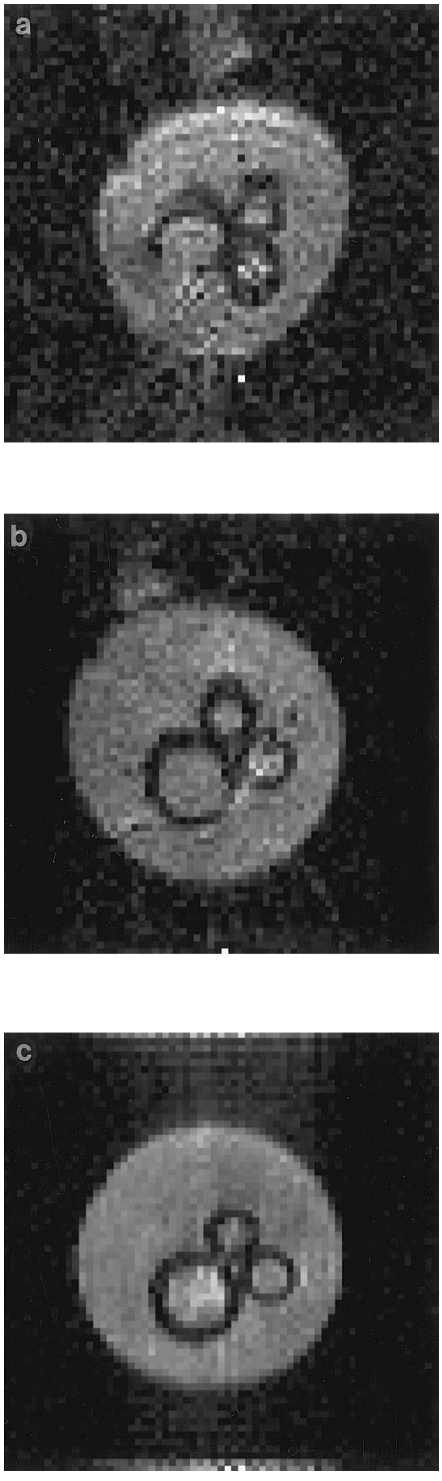

FIG. 6. Single-shot images of a water phantom acquired with (a) MBEST at 1 ms per echo ($G_x = 0.25$ T/m, $\Delta = 128$ μs), (b) MBEST at 0.5 ms per echo ($G_x = 0.5$ T/m, $\Delta = 128$ μs) and (c) PEPI at 1 ms per echo ($G_x = 0.25$ T/m, $\Delta = 128$ μs), showing a progressive reduction in image distortion.

Each switched gradient pulse is separated by a 180° RF pulse, which inverts the phase accumulated by the spins. Once this is taken into account, the read gradient can be treated in a similar way to the switched gradient in MBEST, although the data must be reordered before the PSF is calculated to allow for the manner in which k-space is scanned. The attenuation of the first echo can be written as

$$A_{sw} = \exp\left(\frac{-\gamma^2 D G_x^2}{3}(2\tau^3 + 6\Delta\tau^2)\right). \quad [7]$$

The attenuation of the mth echo is therefore

$$A_{sw} = \exp\left(\frac{-\gamma^2 D G_x^2}{3}(2\tau^3 + 6\Delta\tau^2)(m+1)\right). \quad [8]$$

Equations [6] and [8] can be used to calculate the signal throughout the experiment. As for MBEST, the signal decay

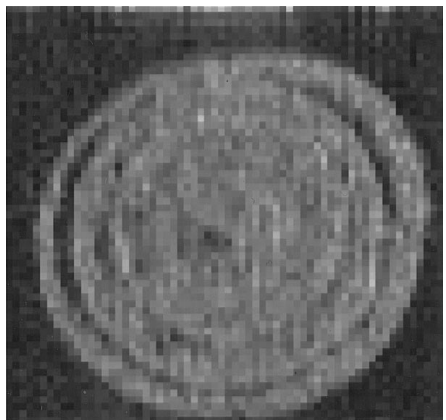

FIG. 7. Single-shot PEPI image of a piece of spring onion in which the rings of tissue are clearly visible. In-plane resolution is 130 μm with a 500 μm slice thickness. Acquisition parameters: $G_x = 0.18$ T/m, $2\tau = 1$ ms, $\Delta = 128$ μs.

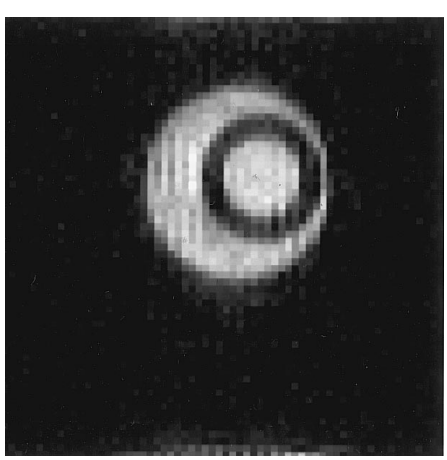

FIG. 8. Single-shot PEPI image of a water phantom of diameter 1.3 mm containing a second tube of inner diameter 0.52 mm and wall thickness 0.14 mm. The in-plane resolution is 50 μm with a 200 μm slice thickness. Imaging parameters: $G_x = 0.5$ T/m, $\Delta = 128$ μs, $2\tau = 1$ ms.

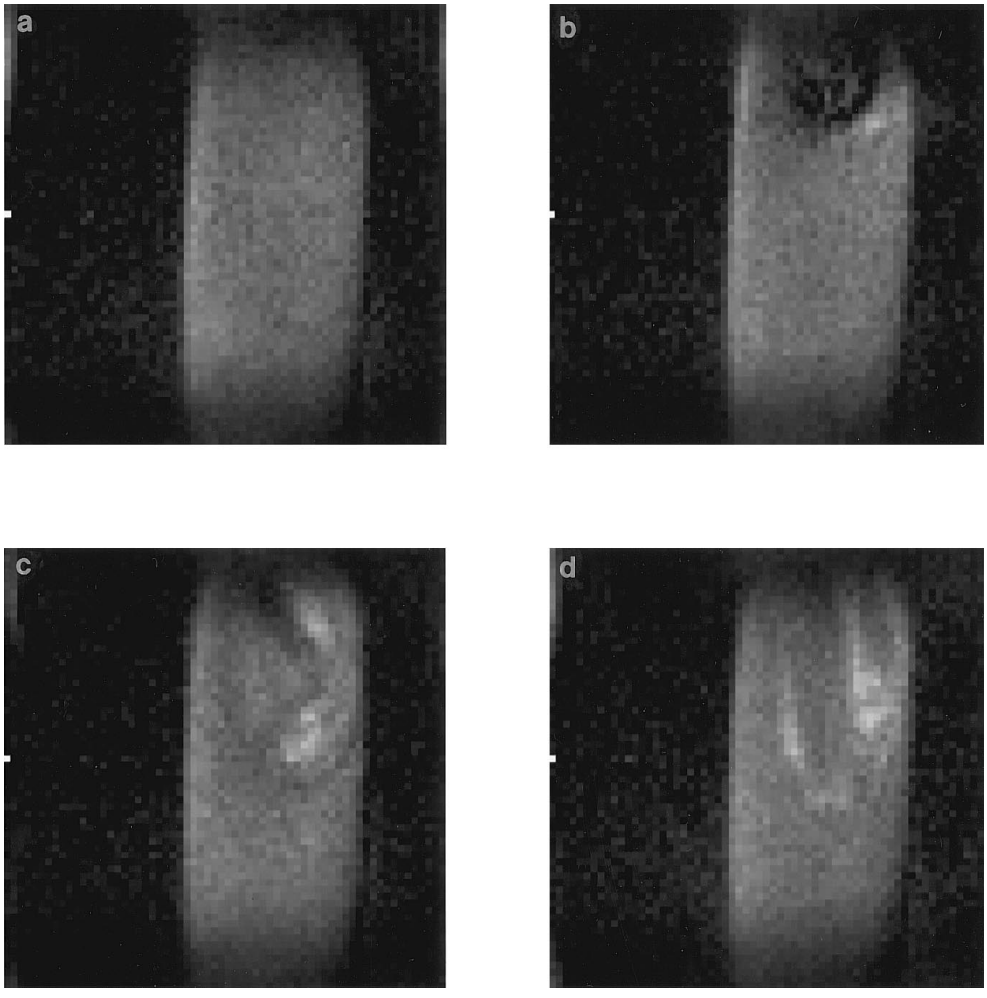

FIG. 9. PEPI images of a drop of water doped with Gd-DTPA falling into a 5 mm NMR tube filled with undoped water at (a) 0 s, (b) 0.6 s, (c) 1.2 s, and (d) 4.5 s after the release. In-plane resolution is 200 μm with a 1 mm slice thickness. Acquisition parameters: TR = 0.3 s, G_x = 0.12 T/m, 2τ = 1 ms, Δ = 128 μs.

increases with the square of the gradient strength and the cube of the experimental duration. Using the previous example of a 64 × 64 image matrix, a switched gradient strength of 0.575 T/m, a phase encoding time Δ = 128 μs, equal resolution in the x and y directions, and a sample of water $D = 2.2 \times 10^{-9}$ m^2s^{-1}), the diffusion limited resolution is 28 μm. The signal decay for this case is shown in Fig. 4. It should be noted that because of the different order of data acquisition, the center of k-space is sampled first, when the signal is still high. This leads to a higher SNR image than is possible with MBEST.

If it is assumed that the maximum gradient strength available is applied with zero gradient rise time, and that both the gradient strength and resolution are equal in the x and y directions, then it is possible to calculate the maximum resolution for any gradient value and diffusion coefficient. Such a graph is shown in Fig. 5, for the PEPI sequence with diffusion coefficients of 2.2×10^{-9} m^2s^{-1} and 1.1×10^{-9} m^2s^{-1}. Since each curve is of the form $1/G^{1/3}$, an increase in available gradient strength leads to a higher achievable resolution, but the rate of change decreases with increasing G.

Image Distortion

The major contribution to image distortion in EPI comes from inhomogeneity of the static magnetic field. Over a small volume, in a well-shimmed magnet, most of the inhomogeneity results from differences in magnetic susceptibility inside and in the vicinity of the sample. For example, if each echo in a 64 × 64 image is acquired in 0.5 ms, and the entire image in 40 ms, then the frequency per point is 2 kHz in the switched direction, but only 25 Hz in the phase encode direction. A static field distortion of greater than 25 Hz (or 0.05 ppm for protons at 11.7 T) will give rise to a distortion in the phase encode direction of more than one pixel.

One method by which image distortion can be reduced is to

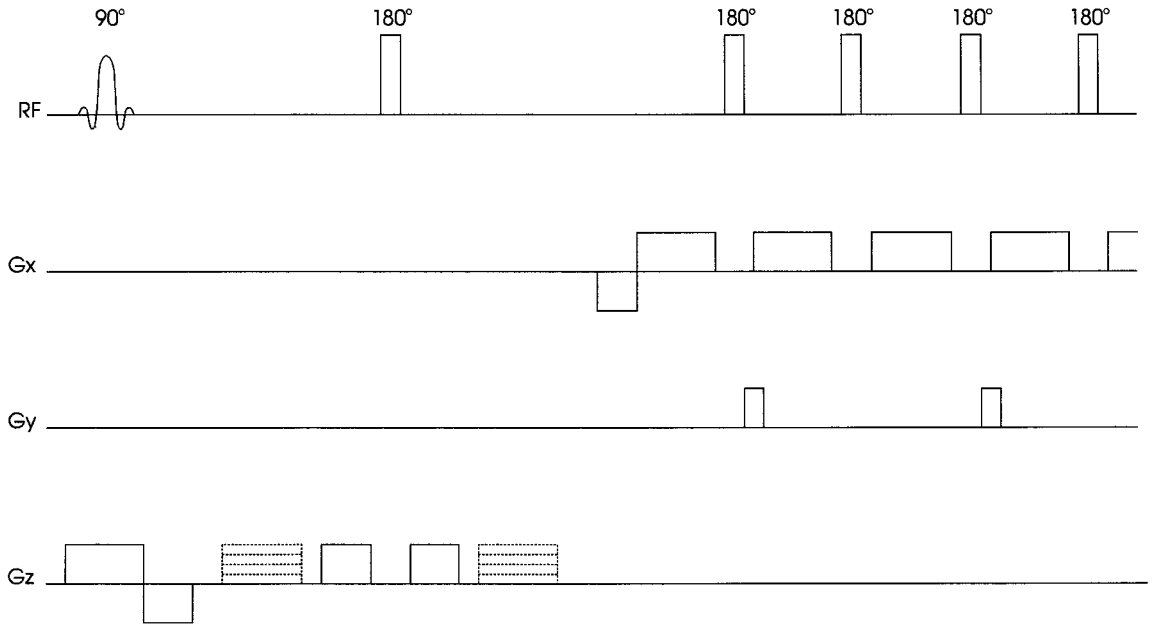

FIG. 10. 3D PEPI sequence as implemented on the microscope system.

decrease the acquisition time. This increases the frequency per point and hence reduces the effect of any static field distortion. However, this is at the expense of an increased sampling bandwidth, which reduces the SNR of the image. In addition, larger gradient strengths are required to achieve a given resolution when the acquisition time is reduced.

The refocusing effect of the 180° RF pulses in the PEPI experiment ensures that there is no phase evolution of the spins due to static magnetic field variations in the phase encode direction. Hence, for an $N \times N$ image, image distortion is reduced by a factor of N compared to the equivalent MBEST experiment.

METHODS

The two sequences described above were implemented on an 11.7 Tesla microscope system (*10*) equipped with actively screened gradient coils (*11*) of 30 mm internal diameter. Because of the sensitivity of MBEST to magnetic field distortion, samples had to be axially symmetric and mounted vertically in the magnet. For this reason, a 14 mm diameter birdcage RF coil was used. As PEPI does not suffer from these effects to the same degree, a solenoidal RF coil could be used for some samples. This gave a better filling factor for small samples and hence better signal-to-noise ratio.

RESULTS

To demonstrate the image distortion caused by magnetic field inhomogeneity, the shim coils in the magnet were switched off and a series of images acquired. Figure 6a shows a 64×64 MBEST image of a water phantom containing three glass tubes, which have outer diameters of 830, 880, and 1400 μm. The resolution is 100 μm in-plane, with a 400-μm slice thickness. This image was acquired at a rate of one echo per millisecond ($2\tau = 1$ ms, $\Delta = 128$ μs, $G_x = 0.25$ T/m), and shows considerable distortion. Figure 6b shows the same phantom imaged at a rate of one echo every 0.5 ms ($2\tau = 0.5$ ms, $\Delta = 128$ μs, $G_x = 0.5$ T/m). The image distortion is reduced in this image, but is still apparent. Using the PEPI sequence, and the longer time of 1 ms per echo ($2\tau = 1$ ms, $\Delta = 128$ μs, $G_x = 0.25$ T/m), the image distortion is reduced still further (Fig. 6c).

The line artifact at the top and bottom of the PEPI image is a result of transverse magnetization generated by imperfections in the train of 180° RF pulses, and normally lies across the center of the image. If these RF pulses are applied with a phase which lies alternately along x and y, the image is shifted by half of the field of view, and so is unaffected by the artifact (*12*) after data reordering.

The insensitivity of PEPI to susceptibility induced image distortion is further demonstrated in Fig. 7, which shows an image through a spring onion with an in-plane resolution of 130 μm and a 500 μm slice thickness, acquired with $\Delta = 128$ μs, $G_x = 0.18$ T/m, and $2\tau = 1$ ms. Here, the rings of tissue are clearly seen despite the presence of air/tissue interfaces.

Figure 8 shows a PEPI image of a phantom consisting of a water-filled tube of outer diameter 1.3 mm, which contains a second tube of inner diameter 0.52 mm and wall thickness 0.14 mm. This image was acquired at 1 ms per echo using a switched gradient strength, G_x, of 0.5 T/m. The in-plane res-

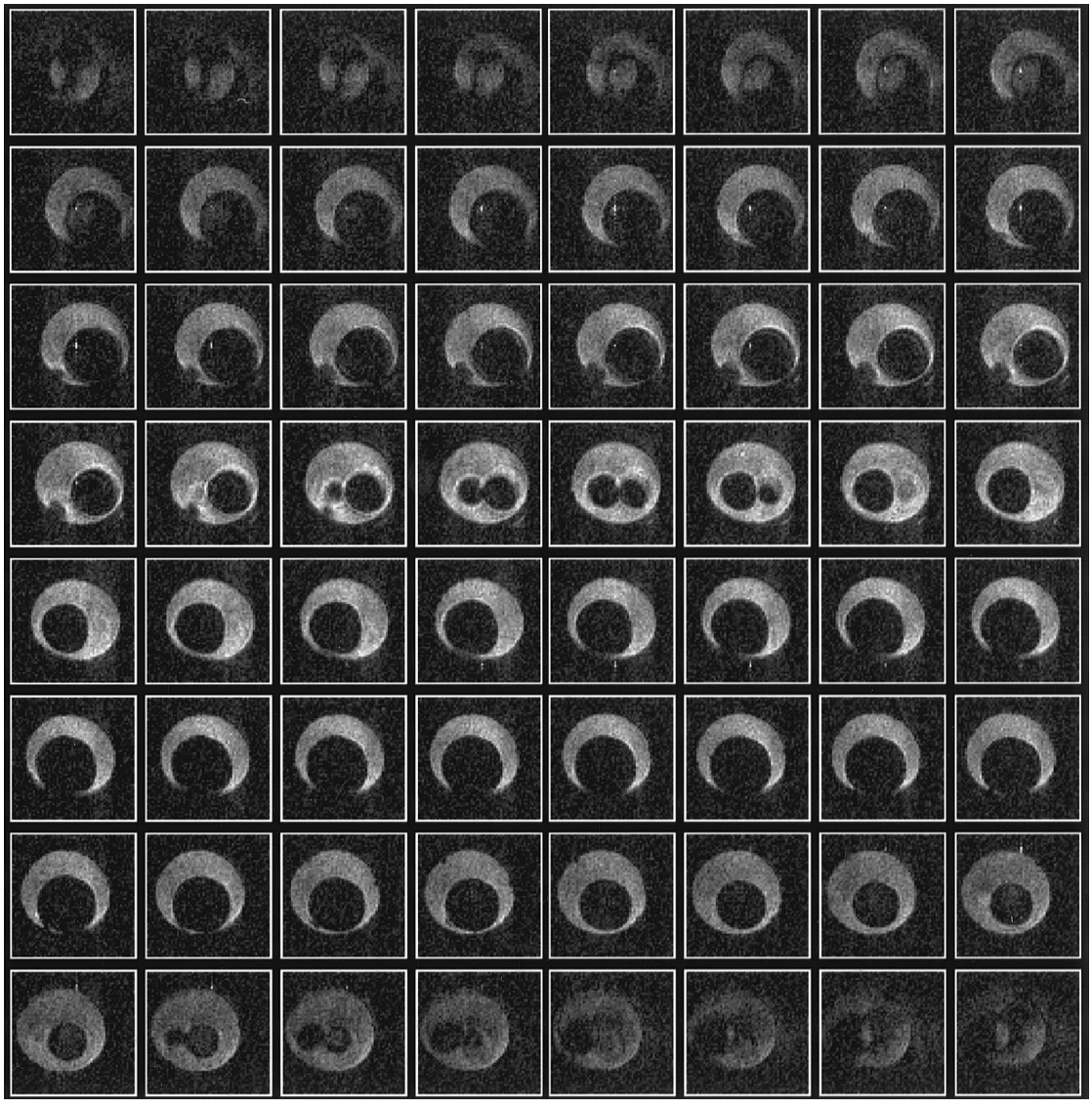

FIG. 11. 3D image of a water phantom filled with glass beads of 3 mm diameter. The matrix size is 64^3 with an isotropic resolution of 100 μm. Acquisition parameters: TR = 1 s, $G_x = 0.25$ T/m, $2\tau = 1$ ms, $\Delta = 128$ μs.

olution is 50 μm, with a 200 μm slice thickness. The SNR in this single-shot image is better than 20:1.

The high-speed nature of PEPI is demonstrated in Fig. 9. A 5 mm diameter NMR tube was filled with distilled water and mounted vertically in the magnet. A single drop of water which had been doped with contrast agent (GD-DTPA) was then allowed to fall into the tube. Since high temporal resolution was required, an inversion recovery experiment could not be performed. Instead, the TR was reduced to 0.3 s, and saturation effects were used to visualize the rapid movement of the contrast agent. Figure 9a shows the tube of water before the entry of the drop. In Fig. 9b, a void is seen at the top of the tube as the drop enters the water. Figures 9c and 9d show the spreading out of the drop which appears bright due to its shorter T_1. The in-plane resolution in these images is 200 μm, with 1 mm slice thickness ($G_x = 0.12$ T/m, $2\tau = 1$ ms, $\Delta = 128$ μs).

3D IMAGING WITH PEPI

By applying a phase encode gradient along the same axis as the slice selection, the PEPI technique can easily be extended to three dimensions (*7*). While this is no longer a single-shot technique, an $N \times N \times N$ image may be acquired in only N excitations. The sequence as implemented on the microscope system is shown in Fig. 10. The 180° RF pulses now have a more complicated effect on the order of data acquisition, moving the k-space coordinate from (k_x, k_y, k_z) to $(-k_x, -k_y, -k_z)$ at the end of each echo. After suitable reordering of the data, each k_z-plane of data comes from two excitations having

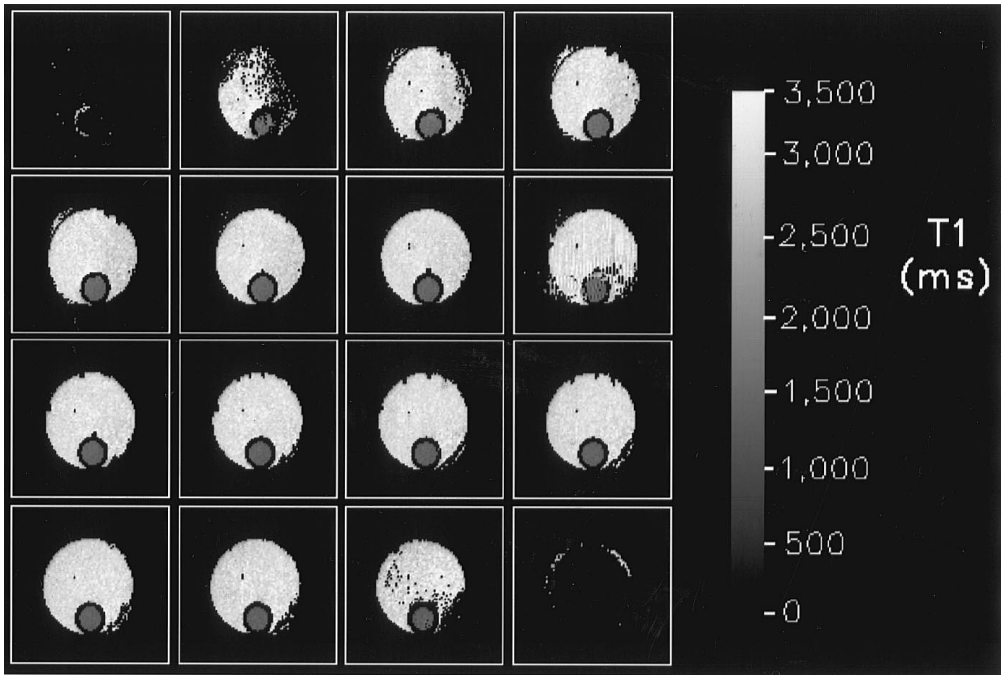

FIG. 12. 3D T_1 measurement by inversion recovery PEPI. The outer tube contains distilled water. The inner tube contains water doped with contrast agent which shortens T_1. The resolution is 80 μm in each direction. Acquisition parameters: TR = 10 s, TI = 1 to 4000 ms, $G_x = 0.30$ T/m, $2\tau = 1$ ms, $\Delta = 128$ μs.

opposite signed phase encoding. If there is any asymmetry in the gradients, then these two data sets will not match, leading to artifacts in the image. Such asymmetry may result from DC offsets in the gradient amplifiers, or incorrect refocusing of the magnetization following slice selection. It was found that splitting the phase encoding gradient so that it was stepped from a maximum value to zero before the 180° RF pulse, and then from zero to the maximum value after the RF pulse, made the sequence much easier to set up, since the symmetry of the phase encoding was guaranteed.

Using this technique, rapid volumar imaging is possible. Figure 11 shows a 3D image of a water-filled tube containing spherical glass beads of 3 mm diameter. The image matrix consisted of 64^3 pixels and the resolution was 100 μm in each direction. The complete image was acquired in 64 s using a repetition time (TR) of 1 s, $G_x = 0.25$ T/m, $\Delta = 128$ μs, and $2\tau = 1$ ms.

By preceding each excitation with a 180° RF pulse, a series of 3D inversion recovery images may be obtained, from which volumar maps of T_1 can be calculated. To assess the accuracy of this measurement, a phantom which consisted of a capillary tube within a 5 mm NMR tube was built. The larger tube was filled with water, while the inner tube contained water doped with contrast agent (Gd-DTPA). A set of 14 3D images were then acquired with inversion recovery times between 1 ms and 4 s. The matrix size was $128 \times 128 \times 16$ with an isotropic resolution of 80 μm. Using a TR of 10 s to avoid any saturation effects, the data set was obtained in 40 min. Using a standard spin echo experiment with the same TR would have taken more than 3 days. The resulting T_1 map, produced using a two parameter fit to the data, is shown in Fig. 12. A spectroscopy experiment was performed on bulk samples of the two liquids. The T_1 of the water was found to be 2.72 ± 0.07 s, while the T_1 of the doped water was 1.21 ± 0.02 s. This compared well with the results from the imaging, which were 3.17 ± 0.15 s and 1.36 ± 0.10 s, respectively.

CONCLUSIONS

Both MBEST and PEPI sequences have been implemented on an 11.7 T NMR microscope. The point spread functions, resulting from the effects of diffusion, of each sequence have been calculated and it has been shown that true microscopic resolution may be achieved with reasonable gradient strengths using both sequences. PEPI has been used to generate images with an in-plane resolution of up to 50 μm, which is approaching the diffusion limit set by the gradient strengths available on our microscope.

PEPI has been extended to three dimensions, allowing the acquisition of three-dimensional images with microscopic resolution. This technique has been further extended to produce volumar T_1 maps in a few minutes. We have now applied PEPI microscopy to the measurement of flow and relaxation times in porous rock samples (*13*).

The relative insensitivity of PEPI to magnetic field inhomogeneity, in comparison to MBEST, makes it the better single-shot sequence for use at high magnetic field. In addition, the early acquisition of the center of *k*-space gives improved SNR.

However, the high level of RF power may limit the use of PEPI for the study of living systems.

REFERENCES

1. P. Mansfield, Multi-planar image formation using NMR spin echoes, *J. Phys. C* **10,** L55 (1977).
2. P. Mansfield and P. G. Morris, "NMR Imaging in Biomedicine," Academic Press, New York (1982).
3. R. J. Ordidge, R. Coxon, B. Chapman, R. Turner, M. Stehling, and P. Mansfield, Snapshot head imaging at 0.5 T using the echo-planar technique, *Magn. Reson. Med.* **8,** 110 (1988).
4. M. K. Stehling, A. M. Howseman, R. J. Ordidge, B. Chapman, R. Turner, R. Coxon, P. Glover, P. Mansfield, and R. E. Coupland, Whole-body echo planar M R imaging at 0.5 T, *Radiology* **170,** 257 (1989).
5. D. N. Guilfoyle, P. Mansfield, and K. J. Packer, Fluid flow measurement in porous media by echo-planar imaging, *J. Magn. Reson.* **97,** 342 (1992).
6. D. N. Guilfoyle and P. Mansfield, Fluid flow measurement in porous media by echo-planar imaging, *Magn. Reson. Imag.* **9,** 775 (1991).
7. D. N. Guilfoyle, B. Issa, and P. Mansfield, Rapid volumetric NMR imaging of fluids in porous solids using a 3D PI-EPI (PEPI) hybrid, *J. Magn. Reson. A* **119,** 151 (1996).
8. P. T. Callaghan and C. D. Eccles, Diffusion limited resolution in NMR microscopy, *J. Magn. Reson.* **78,** 1 (1998).
9. C. B. Ahn and Z. H. Cho, A generalized formulation of diffusion effects in μm resolution magnetic resonance imaging. *Med. Phys.* **16,** 22 (1989).
10. R. W. Bowtell, G. D. Brown, P. M. Glover, M. McJury, and P. Mansfield, Resolution of cellular structures by NMR microscopy at 11.7 T, *Phil. Trans. Roy. Soc. Lond. A* **333,** 457 (1990).
11. P. Mansfield and B. Chapman, Multishield active magnetic screening of coil structures in NMR, *J. Magn. Reson.* **72,** 211 (1986).
12. F. Hennel, Modification of the Carr–Purcell sequence for single-shot echo-planar imaging, *Magn. Reson. Med.* **26,** 116 (1992).
13. A. M. Peters, P. S. Robyr, R. W. Bowtell, and P. Mansfield, Echo planar microscopy of porous rocks, *Magn. Reson. Imag.* **14,** 875 (1996).